Journal of Geophysical Research - Solid Earth
FEB 15 2007; 112 (B2) NIL_78-NIL_84
http://dx.doi.org/10.1029/2006JB004527

An edited version of this paper was published by AGU.

Comment on "Excess pore pressure resulting from methane hydrate dissociation in marine sediments: A theoretical approach" by Wenyue Xu and Leonid N. Germanovich

Nabil Sultan

IFREMER, Département Géosciences Marines, Plouzané France ; nabil.sultan@ifremer.fr

Abstract:

While it is well accepted that gas hydrate dissociation at the base of the Gas Hydrate Stability Zone (*GHSZ*) can generate high excess pore pressure and leads to sediment deformation, the consequence in terms of pore pressure of the dissolution of the gas hydrate at the top of the Gas Hydrate Occurrence Zone (*GHOZ*) remains neglected. The purpose of this comment on *Xu and Germanovich* [2006] article is to demonstrate that gas hydrate dissolution in the *GHSZ* may generate excess pore pressure and to point out the risk related to hydrate dissolution at the top of the *GHOZ*.

Keywords: Dissociation, dissolution, hydrate, pore pressure

Introduction

Parameters affecting gas hydrate formation and dissociation include temperature, pore pressure, gas chemistry, and pore-water salinity. Any change in the equilibrium of these parameters may result in dissociation and/or dissolution of the gas hydrate. While it is well accepted that gas hydrate dissociation at the base of the *GHSZ* can generate high excess pore pressure and leads to sediment deformation, the consequence in terms of pore pressure of the dissolution of the gas hydrate at the top of the *GHOZ* remains neglected. Recently, *Sultan et al.* [2004] theoretically evaluated, for confined pore spaces, the excess pore pressure generated by the hydrate dissolution in the *GHSZ* and the hydrate dissociation at the base of the *GHSZ*. *Sultan et al.* [2004] have also considered the dissipation of the excess pore pressure with time by considering the hydraulic diffusivity of the sediment and using the Darcy's law. Due to the lack of experimental data on the formation and dissolution of methane hydrate from single-phase aqueous solutions, *Sultan et al.* [2004] have shown experimental data [from *Zhang*, 2003] of CO_2 hydrate dissolution to illustrate, and not as a proxy for methane hydrate dissolution as mentioned by *Xu and Germanovich* [2006], the process of pore pressure generation generated by hydrate dissolution. More recently, *Xu and Germanovich* [2006] have presented a similar theoretical approach to quantify the excess pore pressure generated by the methane hydrate dissociation at the base of the *GHSZ* by neglecting the effect of the pressure and temperature changes on the gas solubility. On the other hand, for the hydrate dissolution phenomenon, they stated that "*In general, no free gas is produced during the course of gas hydrate dissolution and, since the density of methane hydrates is lower than that of the coexistent liquid water-gas solution, gas hydrate dissolution does not result in excess pore pressure in natural environments*". This statement about hydrate dissolution is incorrect. The *Xu and Germanovich* [2006] statement is based on the mass density differences between liquid water-gas solution and the solid hydrate phase without any consideration of the conservation of mass of the system. The purpose of this comment is to demonstrate that gas hydrate dissolution in the *GHSZ* may generate excess pore pressure and to point out the risk associated to hydrate dissolution at the top of the *GHOZ*.

Hydrate dissociation/dissolution and pore pressure

From general thermodynamic principles, the volume change during hydrate formation out of methane in solution, ΔV, is tied to the variation of methane solubility, S_{CH4}, [*Miller*, 1974; *Handa*, 1990; *Henry et al.*, 1999].

$$\left(\frac{\partial \ln S_{CH4}}{\partial P}\right)_T = \frac{\Delta V}{RT} \qquad [1]$$

where T is the temperature, P is the pressure in the liquid phase and R is the gas constant. Parameters used in this work are listed in Table 1.

Since the initial work by *Miller* [1974], several authors used thermodynamic models to compute methane solubility in a solution at equilibrium with hydrate. All these studies considered the volume change during hydrate formation out of methane in solution and all found a negative volume change, implying a decrease of solubility with increasing pressure at constant temperature [*Handa*, 1990; *Zatsepina and Buffett*, 1997, 1998; *Henry et al.*, 1999].

In the *GHSZ*, methane hydrate dissolution generates water and dissolved methane. The mass density of the water forming the hydrate phase increases with dissolution while the mass density of the surrounding water system decreases. In Table 2 is presented an example of a close system where at the initial time the System#1 contains N mol of pure water and methane

hydrate solid (structure 1) formed by $N.S_{CH_4}$ mol of methane. The system#1 is not at equilibrium and the hydrate solid will be dissolved totally in the pure water in order to reach equilibrium (System#2). The mass densities and volumes of the system#1 and System#2 are presented in Table 2.

Figure 1 presents as a function of depth and the hydrostatic pressure the methane solubility S_{CH_4} in the water solution (-a), the ratio of water to methane n_k in the hydrate phase (-b), the hydrate fraction η in the initial system#1 (-c) and mass densities of the system#1 and system#2 (-d). Data presented in Figure 1 are determined for the methane hydrate equilibrium temperature. The temperature varies from 276.8 K at 400 m of water depth to 296.4 K at around 3000 m of water depth.

From Table 2 and Figure 1 one can see clearly that dissolution of the methane hydrate in a closed system leads to a decrease of the mass density and therefore to an increase of the pore pressure. In Figure 1-d, the mass density differences between System#1 and System#2 is increasing with depth due to the increase of the methane solubility with pressure and temperature. For a water compressibility of 5 10^{-7} kPa^{-1}, the mass density differences between System#1 and System#2 can generate a considerable excess pore pressure (around 4000 kPa at 2000 m of water depth). In the natural environment, the low rate of temperature increase and the pore pressure dissipation generate obviously lesser excess pore pressure. The excess pore pressure generated by gas hydrate dissolution in a porous media with a porosity of 0.52 was shown by *Sultan et al.* [2004] to be low (38 kPa at around 60 m below the seafloor) and not "*considerable*" as stated by *Xu and Germanovich* [2006].

The example illustrated in Figure 1 has to be considered as an upper bound in terms of pore pressure generation, but it is still a clear demonstration of the excess pore pressure generated by hydrate dissolution. In nature, the water in equilibrium with hydrate is at or near the saturation limit with respect to methane. Any subsequent temperature increases will result only in small changes in solubility and correspondingly small changes in mass density and pore pressure resulting from limited hydrate dissolution.

The excess pore pressure Δu generated by hydrate dissolution in a close system can be derived from the following equation:

$$\frac{\Delta u.\kappa(\eta,\phi)}{\phi.\Delta\eta} = A(n_k) \qquad [2]$$

where the system compressibility $\kappa(\eta,\phi)$ depends on the hydrate fraction η and the porosity ϕ, $\phi.\Delta\eta$ is the hydrate volume dissolution and *A(nk)* is the volume expansion factor generated by the hydrate dissolution and it depends on the ratio of water to methane n_k in the hydrate phase. Figure 2 shows the variation of *A(nk)* for three different values of *nk*. As a demonstration, we will consider the example presented by *Sultan et al.* [2004]. With a temperature increases of around 3°C, the water solubility increases by around 4.10^{-4} *mol* CH_4*/mol* H_2O (Figure 1-a) leading to a hydrate fraction decrease $\Delta\eta$ of around 0.013 [from *Sultan et al.*, 2004; Figure 6]. For a porosity of 0.52, n_k of 6.25 and a compressibility of 5.10^{-7} kPa^{-1} [*Xu and Germanovich, 2006;* Figure 2], the excess pore pressure calculated using equation 2 is equal to 784 kPa. By considering the continuous dissipation of the pore pressure coupled to the slow rate of temperature increase, the excess pore pressure presented by *Sultan et al.* [2004] is 20 times lower than the value calculated for a close confined environment.

The excess pore pressure generated by the same hydrate-fraction dissociation (0.013) can be evaluated using the following equation:

$$\Delta u = \int_0^{\Delta\eta} \frac{Rv(n_k,P,T)}{\kappa(Sg,\phi,P,T)} . \phi . d\eta \qquad [3]$$

where the system compressibility $\kappa(Sg,\phi,P,T)$ depends on the pressure *P*, the temperature *T*, the gas fraction *Sg* and the porosity ϕ and $Rv(n_k,P,T)$ is the volume expansion factor generated by the hydrate dissociation and it depends on the pressure *P*, the temperature *T* and n_k. In Figure 2 is presented the variation of the coefficient $Rv(n_k,P,T)$ as a function of depth for three different values of n_k. From Figure 2, one can see clearly the important deviation between the volume expansion factor generated by the hydrate dissolution and the hydrate dissociation. However, by considering a temperature increases of 3°C at the base of the *GHSZ* (1400 mbsf), for n_k of 6.25 the excess pore pressure generated by the dissociation of the 0.013 hydrate fraction is equal to 2700 kPa, only 3.5 times higher than the pore pressure generated by the hydrate dissolution. For a confined environment and a seafloor temperature changes, the effect of the pore pressure in terms of hazards between the top of the *GHOZ* and the bottom of the *GHSZ* becomes equivalent since 1) the temperature increase rate is higher at the top of the *GHOZ* than at the bottom of the *GHSZ* and 2) the effective stress is lower at the top of the *GHOZ* than at the bottom of the *GHSZ*. It is also important to mention that the hydrate stability law bound the excess pore pressure generated by hydrate dissociation at the base of the *GHSZ*. Therefore, for a natural temperature increase the amount of the excess pore pressure is very limited at the base of the *GHSZ* since any pore pressure increases generated by hydrate dissociation will bring the gas-hydrate to a metastable equilibrium and impede the dissociation process.

In natural environment, the importance of the pore pressure generated by hydrate dissolution and dissociation depends on the temperature increase rate and on ratio of thermal diffusivity to hydraulic diffusivity. For a slow rate of temperature increase and a thermal diffusivity 2 to 3 orders of magnitude higher than the hydraulic diffusivity, the excess pore pressure generated by both hydrate dissolution and hydrate dissociation is expected to be low [*Sultan et al.*, 2004]. However, hydrate dissolution and dissociation may significantly alter the structure and mechanical properties of the marine sediments and the subsequent softening and decrease of the shear strength is probably the main driving factor of sediment deformations and slope instabilities.

Hydrate dissolution and shear strength

The effect of the hydrate formation on the increase of the shear resistance of hydrate-bearing sediments is now experimentally well recognized [*Winters et al.*, 2004; *Yun*, 2005]. The increase of the shear resistance depends mainly on the gas hydrate distribution (disseminated in the pores versus cementing grains) and the gas hydrate fraction. The increase of the shear resistance is optimal when gas hydrate acts as a cementing agent between grains.

N. Sultan (manuscript in preparation, 2006) has recently carried out in-situ *CPT* (Cone Penetration Testing) measurements in hydrate-bearing sediments. In-situ mass density using a source of Cesium 137 was also acquired. Figure 3-a and Figure 3-b show the Top of the *GHOZ* at around 3 m below the seafloor which is characterized by a decrease of the mass density of the hydrate-bearing sediments and an important increase of the cone resistance *qt*. From the mass-density and the cone resistance *qt*, it was possible to calculate the hydrate fraction η and the internal friction angle φ (°).Figure 3-c shows clearly the effect of the hydrate fraction on the increase of the internal friction angle and demonstrates that the important increase of the internal friction angle occurred at low hydrate fraction (< 2%).

Results from Figure 3 confirm that in the present case, the gas hydrate acts as a cementing agent between grains and is not disseminated in the pores.
For hydrate cementing grains, the phenomenon of hydrate dissolution in the *GHSZ* is probably similar to destructuration and softening of natural clay. Several authors have shown experimentally an important deformation due to the destructuration of natural clay [*Burland*, 1990; *Leroueil and Vaughan*, 1990]. Yun [2005] has observed that sediment with only 2% of cemented material may collapse under mechanical loading.
Figure 4 schematically presents in a ε_v-*ln* σ_v diagram (ε_v: volumetric strain and σ_v: vertical effective stress) a possible mechanical history of hydrate-bearing sediment. The hydrate first occurred at a depth *z1* below the seafloor under a vertical effective stress σ_{v1} and the sediment is characterized by an undrained shear strength *Su1*. The hydrate formation impedes the normal consolidation of the sediment along the *NCL* (normally consolidated line) due to the rigidity and stiffness of the cementing agent. The hydrate occurrences and the small sediment consolidation increase the sediment shear strength from *Su1* to *Su2*. The subsequent dissolution of the gas hydrate at the top of the *GHOZ* generated by a temperature increase may lead to an important plastic deformation (collapse) of the sediment due to the loss of cementation and the important decrease of the shear resistance (Figure 4). In this schematic behavior of long-term hydrate-bearing sediment, the excess pore pressure generated by the hydrate dissolution is secondary and slope failures are mainly triggered by localized shear strain at the top of the *GHOZ* and the creation of shear discontinuities. The mechanism presented in Figure 4 and the localized shear strains are compatible with the retrogressive failure of the Storegga slide described by *Kvalstad et al* [2005]. Due to the lack of mechanical experimental data on hydrate-bearing sediment after dissolution and dissociation of the gas hydrate the mechanism presented in Figure 4 is of course theoretical and needs validation. In the paper by *Sultan et al.* [2004], the decrease of the shear strength after the hydrate dissolution is considered through the sensitivity of the sediment, which was enough to initiate slope failures.

Conclusion

In this work, a simple theoretical example was considered to demonstrate that contrary to *Xu and Germanovich* [2006] description, hydrate dissolution generates excess pore pressure. For a close system, excess pore pressures generated by hydrate dissolution and dissociation are in the same order of magnitude. Moreover, in natural environment, the excess pore pressure generated by hydrate dissociation is bounded by the gas hydrate stability law inducing for a natural temperature increase a restricted amount of excess pore pressure at the base of the *GHSZ*.
In natural environment and for a long-term process, the amount of the pore pressure generated by the hydrate dissolution and dissociation depends 1) on the temperature increase rate and 2) on the ratio of thermal diffusivity to hydraulic diffusivity. For a seafloor temperature increase as slow as the rate since the last deglaciation, although the first risky area is the top of the *GHOZ* [*Sultan et al.*, 2004], pore pressure generated by both hydrate dissolution and hydrate dissociation is expected to be low. In this last case, the change of the shear strength is the main driving factor of sediment deformations and slope instabilities. For gas hydrate acting as a cementing agent between grains, hydrate dissolution is probably similar to the destructuration and softening of natural clay and may lead to important localized shear strain, the creation of shear discontinuities and the initiation of slope failures.

Acknowledgement.

I thank Pierre Henry for helpful discussions. Constructive comments by the Associate Editor helped improve the note significantly.

References

Burland, J.B. (1990), On the compressibility and shear strength of natural clays, *Géotechnique, 40(3)*, 329–378.

Handa, Y.P. (1990), Effect of hydrostatic pressure and salinity on the stability of gas hydrates, *J. Phys. Chem*., *94*, 2653-2657.

Henry, P., M. Thomas, and M.B. Clennell (1999), Formation of natural gas hydrates in marine sediments 2. Thermodynamic calculations of stability conditions in porous sediments, *J. Geophys. Res.*, *104*, 23005-23022.

Kvalstad, T.J., L. Andresen, C.F. Forsberg, K. Berg, P. Bryn, and M. Wangen (2005), The Storegga slide: evaluation of triggering sources and slide mechanics, *Mar. Pet. Geol.*, *22*, 245−256.

Lepori, L., and P. Gianni (2000), Partial molar volumes of ionic and nonionic organic solutes in water: A simple additivity scheme based on the intrinsic volume approach, *J. Solution Chem.*, *29*, 405–447.

Leroueil, S., and P.R. Vaughan (1990), The general and congruent effects of structure in natural soils and weak rocks, *Géotechnique, 40(3)*, 467–488.

Miller, S.L. (1974), The nature and occurrence of clathrate hydrates, in *Natural Gases in Marine Sediments*, edited by I.R. Kaplan, pp. 151-177, Plenum, New York.

Sloan, E. D., Jr. (1998), Clathrate Hydrates of Natural Gases, 2nd ed., rev. and expanded, 754 pp., CRC Press, Boca Raton, Fla.

Sultan, N., P. Cochonat, J.-P. Foucher and J. Mienert (2004), Effect of gas hydrates melting on seafloor slope instability, *Marine Geology*, *213*, 379-401.

Van der Waals, J.A. and J.C. Platteeuw (1959), *Adv. Chem. Phys*., *2*, 2-57.

Winters, W.J., I.A. Pecher, W.E. Waite, and D.H. Mason (2004), Physical properties and rock physics models of sediment containing natural and laboratory-formed methane gas hydrate, *American Mineralogist*, *89*, 1221–1227.

Xu, W. and L. N. Germanovich (2006), Excess pore pressure resulting from methane hydrate dissociation in marine sediments: A theoretical approach, *J. Geophys. Res.*, *111*, B01104, doi:10.1029/2004JB003600.

Yun, T.S. (2005), Mechanical and thermal study of hydrate bearing sediments, PhD thesis, 194 pp., Georgia institute of Technology, August.

Zatsepina, O.Y., and B.A. Buffett (1997), Phase equilibrium of gas hydrate: Implication for the formation of hydrate in the deep sea floor, *Geophys. Res. Lett.*, *24*, 1567-1570.

Zatsepina, O.Y., and B.A. Buffett (1998), Thermodynamic conditions for the stability of gas hydrate in the seafloor, *Journal of Geophysical Research, B, Solid Earth and Planets, 103 (10)*, 24127-24139.

Zhang, Y. (2003), Formation of hydrate from single-phase aqueous solutions, internal report, 77 pp., Univ. of Pittsburgh, Pittsburgh.

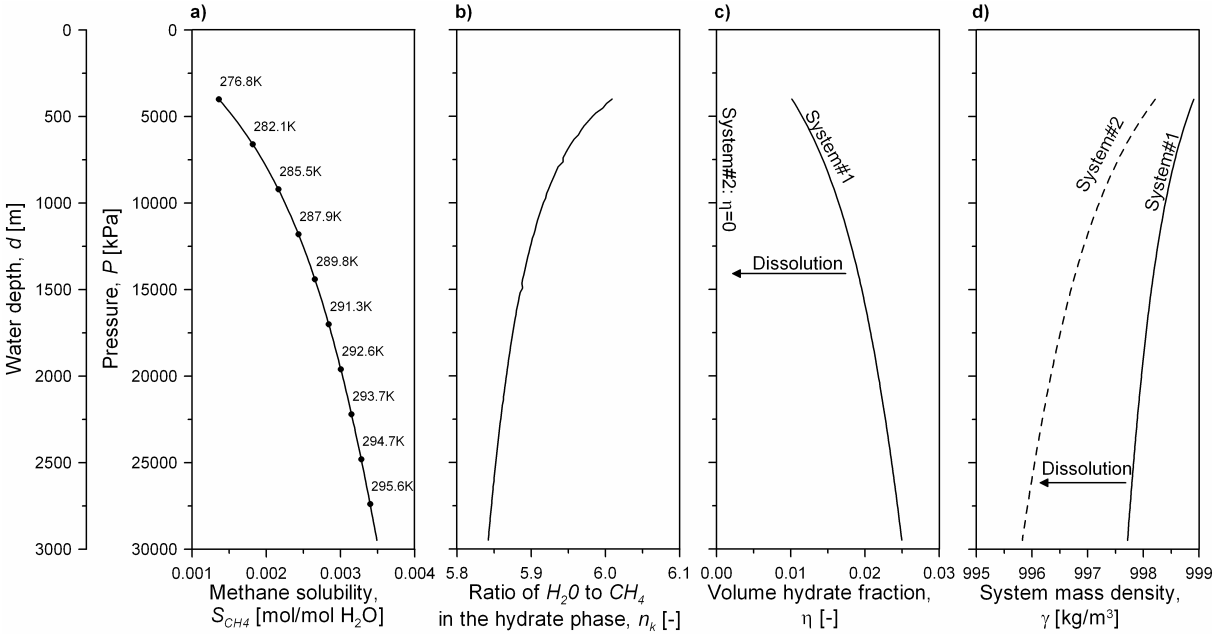

Figure 1. Changes as a function of depth and hydrostatic pressure of a) the methane solubility S_{CH_4} in the water solution, b) the ratio of water to methane n_k in the hydrate phase, c) the hydrate fraction η in the initial system 1 and c) mass densities of the system#1 and system#2. Data are determined for the methane hydrate equilibrium temperature. The mass density of the system containing solid methane-hydrate (system#1) is higher than the system#2 mass density containing water and dissolved methane. The mass density decreases between System#1 and System#2 is at the origin of the excess pore pressure generated by the methane-hydrate dissolution.

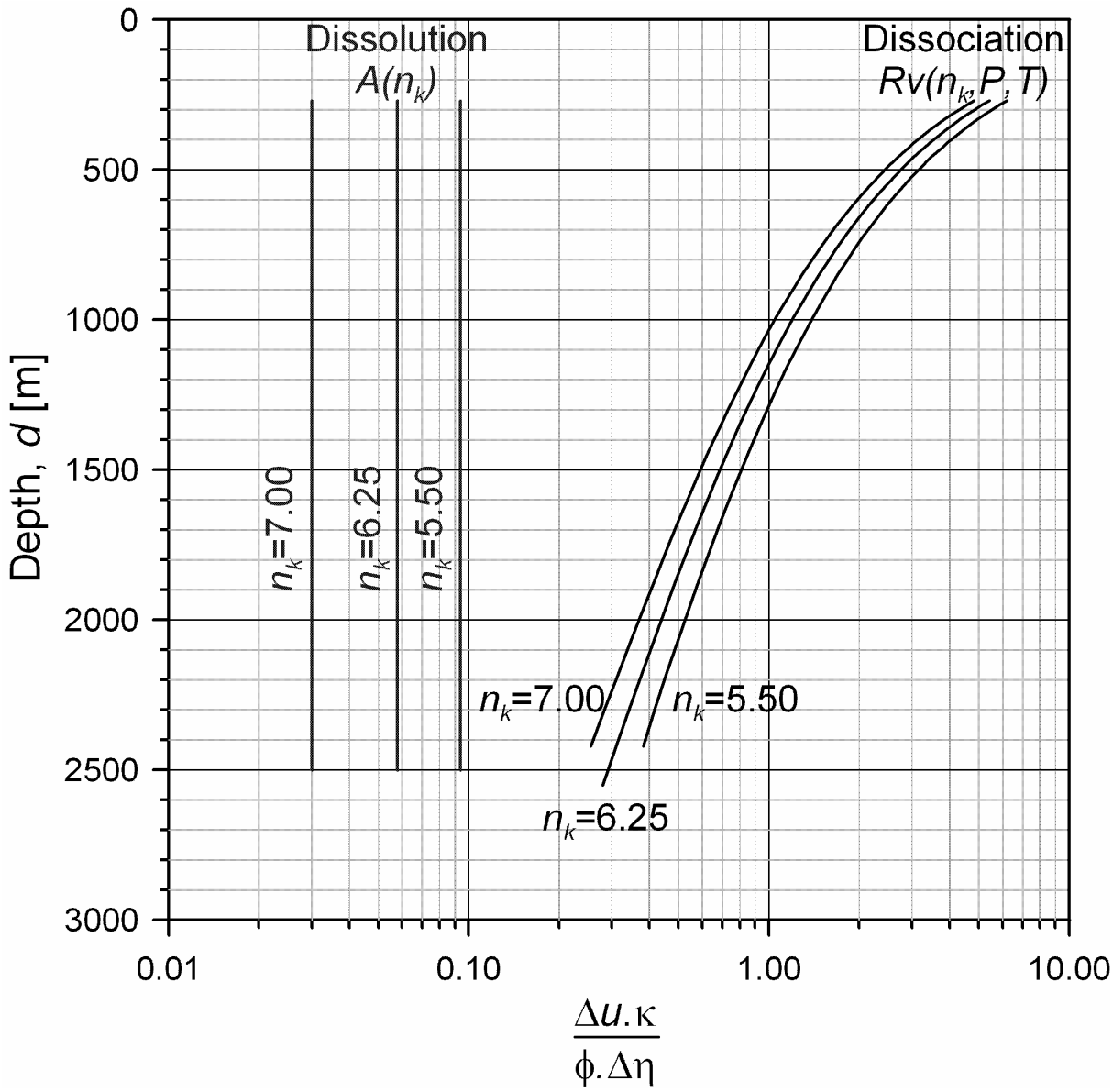

Figure 2. Volume expansion factor for three different ratios of water to methane n_k.

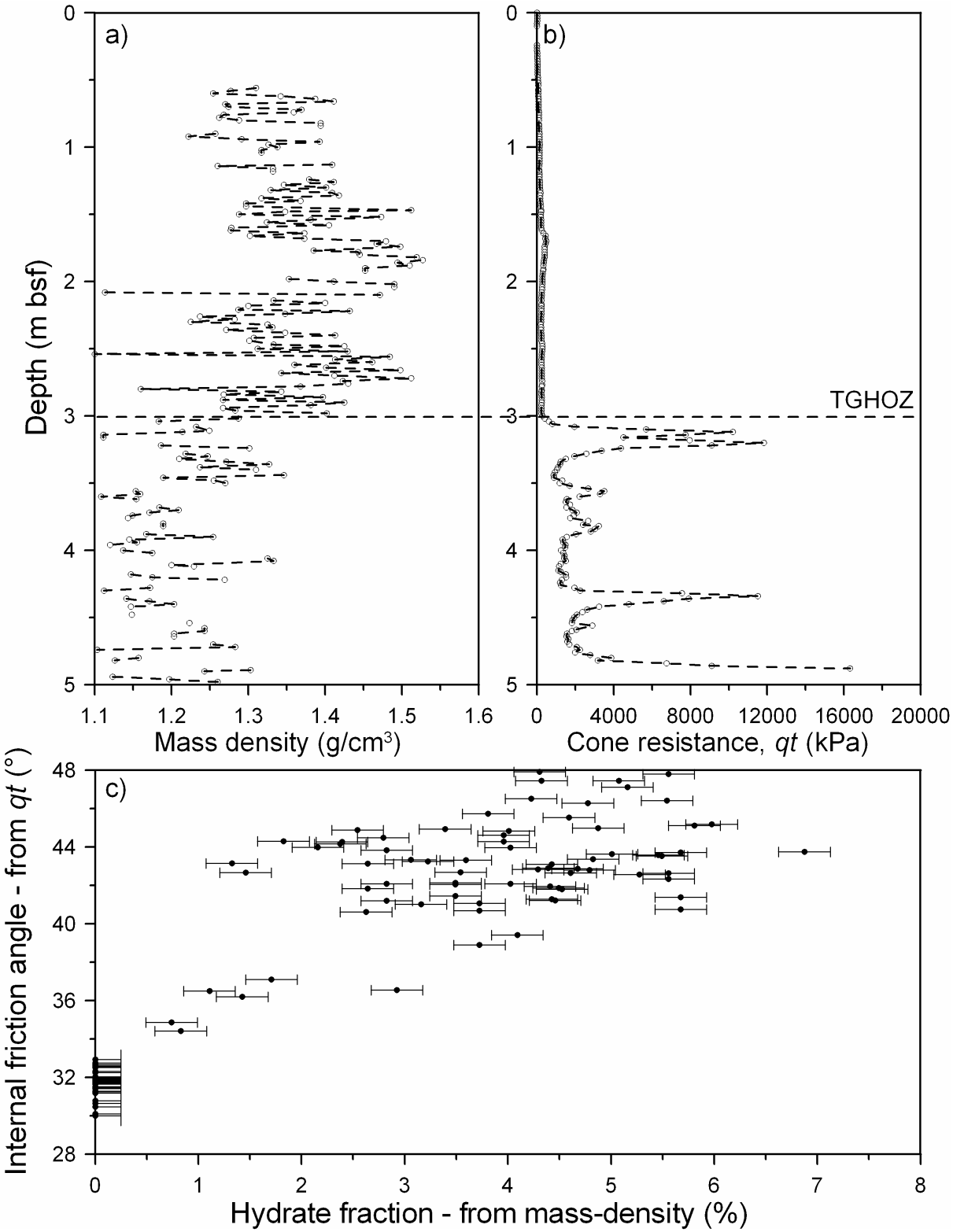

Figure 3. In-situ CPT measurements showing the variation as a function of depth of a) the sediment mass-density and b) the cone resistance qt (N. Sultan, in preparation). c) Hydrate fraction η (calculated from the mass-density of the sediment) as a function of the internal friction angle φ (calculated from the cone resistance qt).

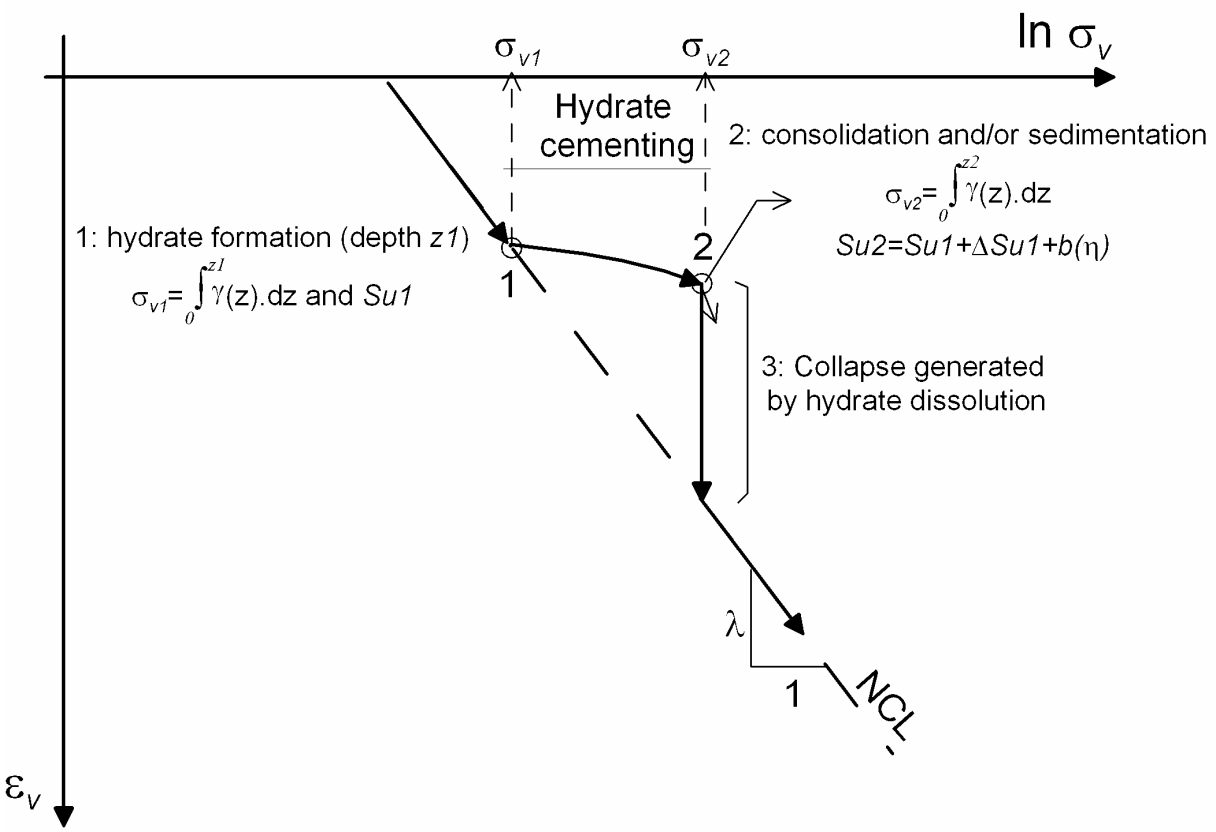

Figure 4. Schematic description of the development of cementing structure in hydrate-bearing sediment which impedes the normal consolidation of the sediment along the NCL (normally consolidated line) and increases the shear strength Su from *Su1* to *Su2* as a function of the hydrate fraction η. The subsequent dissolution of the gas hydrate (pt 3) generates a collapse of the sediment structure (irreversible strain) and an important decrease of the shear strength.

Parameter	Definition
A(nk)	volume expansion factor (under hydrate dissolution)
CPT	Cone Penetration Testing
Δu	excess pore pressure
ΔV	volume change during hydrate formation out of methane in solution
ε_v	volumetric strain
φ	internal friction angle
ϕ	porosity
GHSZ	Gas Hydrate Stability Zone
GHOZ	Gas Hydrate Occurrence Zone
η	hydrate fraction
κ	system compressibility
M_{wl}	molar mass of water
M_{CH4}	molar mass of methane
NCL	normally consolidated line
n_k	ratio of water to methane in the hydrate phase
P	pressure in the liquid phase
qt	cone resistance
$Rv\left(n_k,P,T\right)$	volume expansion factor under hydrate dissociation
R	gas constant
σ_v	vertical effective stress
Sg	free gas fraction
S_{CH_4}	methane solubility in the water solution
Su	undrained shear strength
T	temperature
$\overline{V}_{w1}$	partial molar volume of water in the solution
$\overline{V}_{CH4}$	partial molar volume of methane in the aqueous solution
V_e	volume of the methane-hydrate lattice per mol of water

Table 1. Parameters used in this note.

	System#1: initial conditions			System#2: at equilibrium		
	Mol	**Volume**	**Mass**	**Mol**	**Volume**	**Mass**
Pure water	N	$N.\overline{V}_{w1}$	$N.M_{w1}$	$N+n_k.N.S_{CH_4}$	$\overline{V}_{w1}.N.\left(1+n_k.S_{CH_4}\right)$	$M_{w1}.N.\left(1+n_k.S_{CH_4}\right)$
Dissolved methane	0	0	0	$N.S_{CH_4}$	$N.S_{CH_4}.\overline{V}_{CH4}$	$N.S_{CH_4}.M_{CH4}$
Methane in the hydrate phase	$N.S_{CH_4}$	$V_e.n_k.N.S_{CH_4}$	$N.S_{CH_4}.M_{CH_4}$	0	0	0
Water in the hydrate phase	$n_k.N.S_{CH_4}$		$N.n_k.S_{CH_4}.M_{w1}.$	0	0	0
TOTAL		$N\left[\overline{V}_{wl}+V_e.n_k.S_{CH_4}\right]$	$N.\left[M_{wl}+S_{CH4}\left(M_{CH4}+M_{wl}.n_k\right)\right]$		$N.\left[\overline{V}_{w1}.\left(1+n_k.S_{CH_4}\right)+S_{CH_4}.\overline{V}_{CH4}\right]$	$N.\left[M_{wl}+S_{CH4}\left(M_{CH4}+M_{wl}.n_k\right)\right]$
System Mass density	$\dfrac{M_{wl}+S_{CH4}\left(M_{CH4}+M_{wl}.n_k\right)}{\overline{V}_{wl}+V_e.n_k.S_{CH_4}}$			$\dfrac{M_{wl}+S_{CH4}\left(M_{CH4}+M_{wl}.n_k\right)}{\overline{V}_{w1}.\left(1+n_k.S_{CH_4}\right)+S_{CH_4}.\overline{V}_{CH4}}$		

M_{wl} is the molar mass of water (=0.018016 kg/mol)

M_{CH4} is the molar mass of methane (=0.01604 kg/mol)

$\overline{V}_{w1}$ is the partial molar volume of water in the solution (=1.802 10^{-5} m^3/mol)

$\overline{V}_{CH4}$ is the partial molar volume of methane in the aqueous solution (=3.7 10^{-5} m^3/mol: from Lepori and Gianni (2000))

V_e is the volume of the methane-hydrate lattice per mol of water (=2.263 10^{-5} m^3/mol for methane hydrate (SI) - from Sloan (1998): = $\dfrac{\left(1.2\ 10^{-9}\text{m}\right)^3 .\ \dfrac{6.023\ 10^{23}}{\text{mol}}}{46}$)

n_k is the ratio of water to methane in the hydrate phase (function of temperature and pressure: calculated using the Van der Waals and Platteeuw (1959) theory)

S_{CH_4} is the methane solubility in the water solution at T and P (function of temperature and pressure: calculated from Handa (1990))

Table 2. Masses, volumes and mass densities of the initial and final systems (System#1: initial conditions, System#2: at equilibrium).